Nanoscale Advances

ROYAL SOCIETY OF CHEMISTRY

PAPER

View Article Online
View Journal | View Issue

Cite this: *Nanoscale Adv.*, 2023, **5**, 6560

Interaction of gyrotactic moment of microorganisms and nanoparticles for magnetized and chemically reactive shear-thinning fluid with stratification phenomenon

Zubair Hussain,[a] Waqar Azeem Khan,[a] M. Irfan,[b] Taseer Muhammad,[c] Sayed M. Eldin,[d] M. Waqas[ef] and P. V. Satya Narayana*[g]

Nanotechnology has gained substantial attention on account of its vast applications in food manufacturing, heat exchanges, electronic cooling systems, medical treatment, coolant processes, energy production, biotechnology, transportation, biochemistry, nuclear reactors, and metrology. Currently, the phenomenon of bioconvection using nanomaterials has found wide industrial and technical implementations. Contemporary nanofluids are a dynamic source for illuminating heat transport systems related to engineering as well as industrial phenomena. Bioconvection has numerous applications in bio-micro-systems, owing to the augmentation in mass renovation besides collaborating, which are vital complications in diverse micro-systems. This study intended to model and examine an incompressible, unsteady 3D Casson fluid nanofluid with bioconvection on a stretching surface. A model by means of these characteristics is beneficial in applications, such as in nuclear reactors, coolants in automobiles, metallurgical procedures, energy construction, micro-manufacturing, industrial engineering, and geophysical fluid mechanics along with dynamics. The performance of the Brownian motion along with thermophoresis diffusion is assumed through an extraordinary effect of thermal radiation in the temperature equation of the fluid movement. This model was created by using PDE, which was then converted into an ODE system. The somatic behavior of substantial parameters was investigated graphically. Similarly, tables were interpreted to display the effect of the control of physical quantities on the local Nusselt number, local Sherwood number, and motile density. Consequently, it was determined that the temperature of Casson fluid grew exponentially with higher estimates of the magnetic parameter and the thermal Biot number. At the same time, we detected that augmented estimation of the Lewis number decreases the Casson fluid concentration. For growing values of the parameters, Biot number and the stretching parameter, there is a direct reaction for the microorganism profile.

Received 9th June 2023
Accepted 4th September 2023

DOI: 10.1039/d3na00400g

rsc.li/nanoscale-advances

1. Introduction

Recently, nanoparticles have attracted the attention of researchers owing to their growing significance in food, biomaterials, bioengineering, electronic devices, and the mechanical industry. Nanofluids further offer considerable assistance in biomedical sciences. Examples include cancer therapeutics, magnetic resonance, nano-cryosurgery, localized therapy, labeling of cancerous tissues, magnetic resonance imaging (MRI), bacteriostatic activity, and nano-drug delivery. The word nanofluid indicates nanomaterials suspended in a traditional liquid to enhance the joint heat and mass conversion process. It is a well-defined circumstance that in refrigeration and thermal systems, fluids transient over micro-fluidic procedures rely exclusively on heat transfer molecules carried by nanomaterials. Therefore, nanofluid dynamics is the key term that must be involved in all fields related to non-

[a]*Department of Mathematics, Mohi-ud-Din Islamic University, Nerian Sharif, Azad Jammu and Kashmir 12010, Pakistan*
[b]*Department of Mathematical Sciences, Federal Urdu University of Arts, Sciences & Technology, Islamabad 44000, Pakistan*
[c]*Department of Mathematics, College of Science, King Khalid University, Abha, Saudi Arabia*
[d]*Center of Research, Faculty of Engineering, Future University in Egypt, New Cairo, 11835, Egypt*
[e]*NUTECH School of Applied Science and Humanities, National University of Technology, Islamabad 44000, Pakistan*
[f]*Department of Mechanical Engineering, Lebanese American University, Beirut, Lebanon*
[g]*Department of Mathematics, School of Advanced Sciences, Vellore Institute of Technology, Vellore, Tamilnadu, India 632014. E-mail: psatya@vit.ac.in; pvsatya8@yahoo.co.in*

molecular suspension in every way to endeavor for optimal routine. Nanofluid exists as a subgroup of fluid consisting of (1–100) nanometer-sized materials. Choi[1] presented the elementary conception of these nanomaterials using enhanced thermophysical possessions, which has been popularized by many researchers. Buongiorno[2] discussed the seven sliding developments in nanoparticle movement including Brownian motion and thermophoresis effects. The thermal conductivity of nanoparticles is higher than that of conventional liquids. The nanometer-sized solid particles intensify the transportation rate of heat of conventional fluids. The nanofluid has many potential applications for heat conversion, such as in industrial procedures, cooling systems, chiller, temperature reduction, hybrid-energy appliances, refrigerators, microchips, and fuel cells. Today's world is a fast technological world. The cooling of electronic materials is one of the main requirements of the contemporary industry. Today's standard heat transfer fluids cannot offer adequate cooling in industrial processes. Such conditions have led to the development of a present technology called nanotechnology. The practice of nanofluids in place of an extra effective cooling medium in nuclear power plants means that present coolant can be utilized more efficiently to cool hot surfaces. A thermostatic valve is employed to control heat transfer in nanofluid implementations. Its ability to transfer heat quickly can be used for cooling purposes. Oncologists treat cancer patients by inserting medication as well as radiation into a device involving iron-based nanofluid. Nanofluids are used, for example, as a coolant in an extensive range of automatic cooling usages containing vehicle radiators, PC servers, and warm sun-based accumulators. Abu-Nada, and Oztop studied the properties of Cu-water nanofluid,[3] while Shahzad *et al.*[4] considered the entropy concept for the cross nanofluid with radiation. The entropy optimization in the hybrid nanofluid was presented by Khan *et al.*[5] Furthermore, Khan *et al.*,[6] Ali *et al.*,[7] Khan *et al.*,[8,9] and Anjum *et al.*[10] reported the nanofluid behavior in different fluid models.

The bioconvection of nanofluids circumstance is an alternative extraordinary field of research that has many applications, such as in pharmaceutical engineering, sedimentary waterways, micro-fluidics machines, gas-bearing, model construction, lubrication ingredients, fuel, hydrodynamics systems, polymer construction, microbial augmented oil recovery, and hydrodynamics production. The phenomenon of bioconvection occurs owing to the upward swimming of microorganisms in a definite track within the fluid. Consequently, the density of the fluid in the upper part grows causing the drop of microorganisms. They swim back upward and thus proceed with the development of bioconvection. The bioconvection advances through active swimming and the disorganized movement of motile microorganisms that remain denser in comparison with water. Presently, numerous efforts have been undertaken to study the movement of motile gyrotactic microorganisms in fluid flow due to their important applications in biomedicine, fertilizers, ethanol, biofuel, biomicrosystems, and biotechnology. Because of the gathering appropriate to the already stated microorganisms, a dense cover of bacteria appears beside the top exterior of the lighter fluid. Microorganisms transport an organic fluid upstairs happening some way due toward its lower density associated with water. Biochemical nanomaterials are transparent aqueous and non-aqueous fluids containing gyrotactic motile microorganisms, comprising metal-acquired nanomaterials. The term bioconvection was first familiarized by Platt[11] in an extemporaneous evolutionary process in the association of swimming motile microorganisms. Numerous usages of bioconvection by means of microorganisms and nanoparticles in the region of mechanical energy, biosensors, manufacturing, bioinformatics, and biosensors have attained the consideration of scholars in the direction of this field. Owing to the irregular and unsteady configuration, microbes swim in the superior area. When the microbe has nothing on the top surface, the top area becomes unbalanced due to the high layer density. Microbes float unrestrained in the marine environment, for instance, canyons and rivers and ponds along oceans. The idea of nanofluids in bioconvection is to bring into concentration work defining the evolution of burst formation and density stratification performed with the simultaneous edge of self-propelled microorganisms, nanoparticles, besides drag forces. Functioning micro-organisms may comprise gyrotaxis, gravitaxis, and oxytaxis organisms. Supporting gyrotactic microorganisms in the bulk conversion of liquid enrichment nanofluids, mixing on a small scale, fully within microvolumes, and increasing the stability of nanofluids. Biomedical engineering applies the procedure of bioconvection in bioreactors, fuel cell engineering, and diesel fuel products. Lately, various researchers have employed bioconvection as seen from the literature reports. Some of the foremost and contemporary study on the bioconvection of diverse nanofluidic models by gyrotactic microorganisms can be established in the studies of Kuznetsov,[12] Usman,[13] Chu,[14] and Anjum.[15]

In modern applied sciences, such as geothermal engineering, astrophysical bio-fluid, geophysical, and petroleum sectors, the analysis of non-Newtonian fluids, the studies done by Khan *et al.*,[16] Hayat *et al.*,[17] Khan *et al.*,[18–20] Irfan[21,22] and Bhatti *et al.*[23,24] have received significant consideration. The implementations established on non-Newtonian fluids' connection comprise ceramic products, wire coating, certain oils, printing, fiber engineering, and petroleum industries. Modern technological development calls for revolutionary progress in the field of temperature transference. Even with the complications of non-Newtonian fluids, applied theoreticians and manufacturing scientists are connected in non-Newtonian fluid dynamics, subsequently the flow and heat transfer properties of these fluids are significant for abundant systems and diverse applications in pharmacy, chemical engineering, and bio-technology. In summary, non-Newtonian models have a non-linear bounding affiliation between stress and strain rate. The mechanical properties of non-Newtonian fluids, whether they are shear thinness and/or thickness, normal stress variances, and viscoelastic interactions, may not be described using conservation theory; consequently, advanced and operative forecasting is essential. Several fluid models have been proposed to analyze the transportation rate

of heat and mass, among these models Casson model have the wide range of applications. Casson's model is sustained by structural modeling of the reactive nature of solids along with liquid phases for biphasic suspensions. Casson[25] was the leading scientist who exhibited a mathematical model of this class of liquids. Subsequently, many researchers have shifted their considerations to the flow properties of Casson fluids. Several well-known examples of Casson fluids include honey, tomato pastes, jellies, and soups to concentrated fruit extracts. Human blood can also be deliberated as Casson's fluid as many substances, such as fibrinogens, proteins, and globulins, in aqueous disreputable plasmas besides human red blood cells are present in it. It is requested that this rheological model is superior for some liquids than the viscoelastic model. This model is appropriate for chocolate and blood rheology. Casson fluid is the thin shear fluid that is a type of non-Newtonian fluid since it shows an elastic limit. If a shear stress less than the yield stress is provided, the fluids act like solids, *i.e.*, no flows occur and vanish if the shear stresses are greater than the produced stresses. In the thick shear fluid model, it is assumed to have infinite viscosity near which the shear rate vanishes, resulting in pressures lower than no flow and the viscosity vanishes at an infinite shear rate. A Casson fluid sample consists of the bonds or interactions between the liquid and solid phases. When the elastic limit becomes mandatory and is less than the shear stress, Casson fluids perform resembling solids. Casson's model of fluids has become a non-Newtonian fluid for explorers since those applications have a wide scope in energy construction, industrial and biomedical engineering, geo-physical fluid mechanics besides dynamics. Specific investigations of Casson fluid can be found in ref. 26–32.

The novelty of this analysis is to estimate the significance of thermal radiation on the MHD flow of three-dimensional Casson nanofluids with bioconvection in excess of a stretching sheet. Firstly, MHD flow has gained a lot of attention from scholars for the reason that there are various applications in industries along with engineering. For example, in metallurgical procedures, definite practices involve the cooling of many continuous strips by extracting electrically conductive fluids subject to magnetic fields. It allows one to control the speed of cooling to obtain the desired results. Secondly, the use of bioconvection has across-the-board uses in bio-micro and organic structures casing microbial-better-quality oil retrieval structures, enzyme bio-sensors, and bio-machines. The bioconvection presence is interrelated to organic solutions and microbes. Third, the theory of nanofluids is working in a number of engineering uses, including the refrigeration of electronics, the change of solar thermal energy, and refined developed methods. Furthermore, the assessment of Casson liquids has attracted the attention of various researchers owing to their uses in medicinal, biological work, and biomedical sciences. The production ink, shampoos, fluxes, pastes, and mixtures are the few ingredients explaining the non-Newtonian nature.

1. The purpose of this study is to improve the rate of heat and mass transfer by providing activation energy.

2. Besides, the effects of chemical reactions and double stratification conditions are also taken into account.

3. The basic equations of this problem are updated to a dimensionless system by using appropriate transformations.

4. The system of ordinary differential equations is numerically processed using the bvp4c algorithm in the MATLAB computer program.

5. Numerical calculations are acclimated to study the characteristics of essential parameters.

2. Mathematical modeling

Consider an incompressible, unsteady flow of 3D Casson nanofluid over a stretching sheet with bioconvection. In this study, we deliberated double stratification boundary conditions and thermal radiation. Additionally, the aspects of activation energy, chemical reaction, and MHD are assimilated. Thermophoretic and Brownian dispersion are incorporated for the reason of nanoparticles. The velocity constituents ($u = ax$, $v = by$) of Casson nanofluid are reserved beside x and y directions and $T = T_w = T_0 + e_1x$, $C = C_w = C_0 + e_2x$, $N = N_w = N_0 + e_3x$ represent surface temperature, concentration, and microorganism respectively. The diagram of the Casson nanofluid together with gyrotactic motile microorganisms is shown in Fig. 1.

The rheological equation of state for the incompressible and isotropic flow of a Casson nanofluid is given by:

$$\tau_{ij} = \begin{cases} 2\left(\mu_B + \frac{p_z}{\sqrt{2\pi}}\right)e_{ij}, & \pi > \pi_c \\ 2\left(\mu_B + \frac{p_z}{\sqrt{2\pi_c}}\right)e_{ij}, & \pi_c < \pi \end{cases}$$

where (τ_{ij}, e_{ij}, π, μ_B, π_c) denote the shear stress, deformation rate component $(i, j)^{th}$, the product of the component of deformation, yield stress and critical value of $\pi = e_{ij}e_{ij}p_z$, respectively. By using conservation laws, the basic transport equations for the Casson fluid model in vector form are

$$\nabla \cdot V = 0, \tag{1}$$

$$\rho_f(V\cdot\nabla)V = -\nabla p + \nabla\cdot\tau_{ij} + J \times B, \tag{2}$$

$$(\rho c)_p(V\cdot\nabla T) = \nabla\cdot(k\nabla T) + (\rho c)_f\left(D_B\nabla C\cdot\nabla T + \frac{D_T}{T_\infty}\nabla T\cdot\nabla T\right), \tag{3}$$

$$V\cdot\nabla C = D_B\nabla^2 C + \frac{D_T}{T_\infty}(\nabla T\cdot\nabla T) - k_r{}^2\left(\frac{T}{T_\infty}\right)^m (C - C_\infty)\exp\left(-\frac{E_a}{kT}\right), \tag{4}$$

$$V\cdot\nabla N + \frac{W_c b}{(C_w - C_o)}\left(N\nabla^2 C + \nabla C\cdot\nabla N\right) = D_m\nabla^2 N, \tag{5}$$

Underneath these assumptions, the governing boundary layer system of the equations can be assembled for instance:

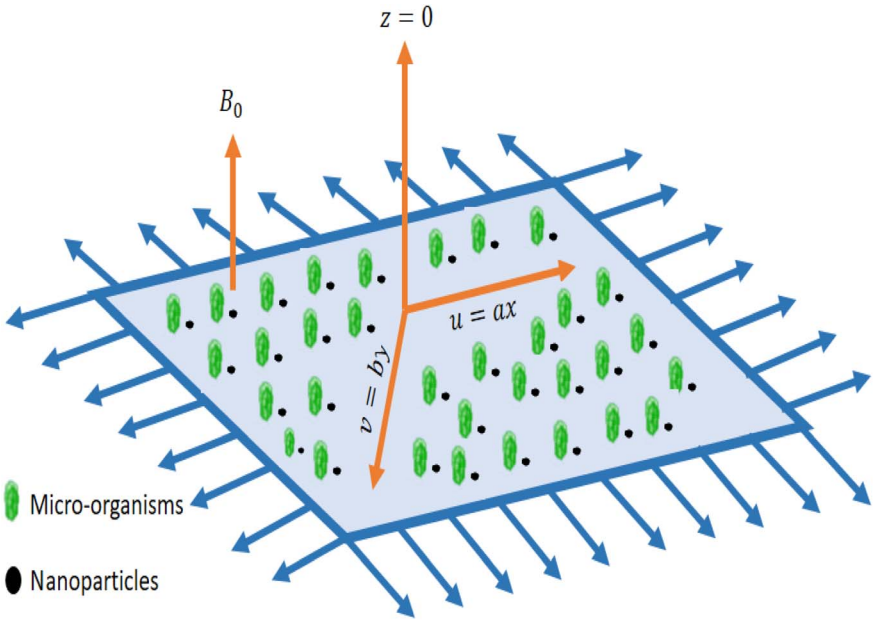

Fig. 1 Physical representation of the flow model.

$$\frac{\partial u}{\partial x}+\frac{\partial v}{\partial y}+\frac{\partial w}{\partial z}=0, \tag{6}$$

$$u\frac{\partial u}{\partial x}+v\frac{\partial u}{\partial y}+w\frac{\partial u}{\partial z}=\upsilon\frac{\partial^2 u}{\partial z^2}\left[1+\frac{1}{\beta}\right]-\frac{\upsilon}{K_p}u-\frac{\sigma^{**}{B_0}^2}{\rho_f}u, \tag{7}$$

$$u\frac{\partial v}{\partial x}+v\frac{\partial v}{\partial y}+w\frac{\partial v}{\partial z}=\upsilon\frac{\partial^2 v}{\partial z^2}\left[1+\frac{1}{\beta}\right]-\frac{\upsilon}{K_p}v-\frac{\sigma^{**}{B_0}^2}{\rho_f}v, \tag{8}$$

$$u\frac{\partial T}{\partial x}+v\frac{\partial T}{\partial y}+w\frac{\partial T}{\partial z}=\alpha_1\frac{\partial^2 T}{\partial z^2}+\tau\left[D_B\frac{\partial C}{\partial z}\frac{\partial T}{\partial z}+\frac{D_T}{T_\infty}\left(\frac{\partial T}{\partial z}\right)^2\right]-\frac{1}{(\rho c)_f}\frac{\partial q_r}{\partial z}, \tag{9}$$

$$u\frac{\partial C}{\partial x}+v\frac{\partial C}{\partial y}+w\frac{\partial C}{\partial y}=D_B\frac{\partial^2 C}{\partial z^2}+\frac{D_T}{T_\infty}\frac{\partial^2 T}{\partial z^2}-{k_r}^2\left(\frac{T}{T_\infty}\right)^m(C-C_\infty)\exp\left(-\frac{E_a}{kT}\right), \tag{10}$$

$$u\frac{\partial N}{\partial x}+v\frac{\partial N}{\partial y}+\frac{\partial}{\partial z}\left(N\frac{\partial C}{\partial z}\right)\frac{W_c b}{(C_w-C_o)}+w\frac{\partial N}{\partial z}=\frac{\partial}{\partial z}\left(D_m\frac{\partial N}{\partial z}\right), \tag{11}$$

with

$$u=U_w=ax, v=V_w=by, w=0, -k\frac{\partial T}{\partial z}=h_f(T_f-T),$$
$$-D_B\frac{\partial C}{\partial z}=h_g[C_f-C\,], -D_m\frac{\partial N}{\partial z}=h_k[N_f-N\,]\ \text{ at }\ z=0, \tag{12}$$

$$u\to 0, v\to 0, \frac{\partial u}{\partial z}\to 0, \frac{\partial v}{\partial z}\to 0, T\to T_\infty=T_0+d_1x,$$
$$C\to C_\infty=C_0+d_2x, N\to N_\infty=N_0+d_3x\ \text{ as }\ z\to\infty. \tag{13}$$

By using the Rosseland approximation, we find the radiative heat flux as,

$$q_r=-\frac{16\sigma^*{T_\infty}^3}{3k^*}\frac{\partial T}{\partial z}. \tag{14}$$

Considering:

$$u=axf'(\eta), v=ayg'(\eta), w=-\sqrt{av}[f(\eta)+g(\eta)], \eta=z\sqrt{\frac{a}{v}},$$
$$\theta(\eta)=\frac{T-T_\infty}{T_w-T_o}, \phi(\eta)=\frac{C-C_\infty}{C_w-C_o}, \chi(\eta)=\frac{N-N_\infty}{N_w-N_o}. \tag{15}$$

We have

$$f'''\left(1+\frac{1}{\beta}\right)-f'^2+f''(f+g)-(M+\lambda)f'=0, \tag{16}$$

$$g'''\left(1+\frac{1}{\beta}\right)-g'^2+g''(f+g)-(M+\lambda)g'=0, \tag{17}$$

$$\left[1+\frac{4}{3}R_d\right]\theta''+\mathrm{Pr}(f+g)\theta'-\mathrm{Pr}f'\theta+\mathrm{Pr}\left[N_b\theta'\phi'+N_t\theta'^2-S_1f'\right]=0, \tag{18}$$

$$\phi'' + \mathrm{Pr}L_e\left[(f+g)\phi' - f'\phi - S_2 f'\right] + \frac{N_t}{N_b}\theta'' - \mathrm{Pr}L_e\sigma[1+\delta\theta]^m\phi\exp\left(\frac{-E}{1+\delta\theta}\right) = 0, \quad (19)$$

$$\chi'' + L_b\chi'[f+g] - L_b(S_3+\chi)f' - P_e[\phi''(\chi+\Omega) + \phi'\chi'] = 0, \quad (20)$$

$$f(0) = 0, f'(0) = 1, f'(\infty) \to 0, \quad (21)$$

$$g(0) = 0, g'(0) = \alpha, g'(\infty) \to 0, \quad (22)$$

$$\theta'(0) = -\gamma_1[1 - S_1 - \theta(0)], \theta(\infty) \to 0, \quad (23)$$

$$\phi'(0) = -\gamma_2[1 - S_2 - \phi(0)], \phi(\infty) \to 0, \quad (24)$$

$$\chi'(0) = -\gamma_3[1 - S_3 - \chi(0)], \chi(\infty) \to 0, \quad (25)$$

where

$$\mathrm{Pr} = \frac{\upsilon}{\alpha_1}, R_d = \frac{4\sigma^* T_\infty^3}{kk^*}, N_b = \frac{\tau D_B(C_w - C_o)}{\upsilon}, N_t = \frac{\tau D_T(T_w - T_o)}{\upsilon T_\infty}, \alpha = \frac{b}{a},$$
$$M = \frac{\sigma^{**}B_0^2}{a\rho_f}, E = \frac{E_a}{\kappa T_\infty}, \delta = \frac{T_w - T_o}{T_\infty}, S_1 = \frac{d_1}{e_1}, S_2 = \frac{d_2}{e_2}, S_3 = \frac{d_3}{e_3}, \lambda = \frac{\upsilon}{aK_p},$$
$$P_e = \frac{bW_c}{D_m}, L_e = \frac{\alpha_1}{D_B}, \gamma_1 = \frac{h_f}{k}\sqrt{\frac{\nu}{a}}, \gamma_2 = \frac{h_g}{D_B}\sqrt{\frac{\nu}{a}}, \gamma_3 = \frac{h_k}{D_m}\sqrt{\frac{\nu}{a}},$$
$$L_b = \frac{\upsilon}{D_m}, \sigma = \frac{k_r^2}{a}, \Omega = \frac{N_\infty}{(N_w - N_o)}. \quad (26)$$

Precisely, expressions for Nusselt and Sherwood numbers (Nu_x, Sh_x) and density of the microbe (Nn_x) in dimensional type are:

$$Nu_x = \left(-\frac{x}{(T_w - T_\infty)}\frac{\partial T}{\partial z} + \frac{xq_r}{(T_w - T_\infty)}\right) \text{ at } z = 0, \quad (27)$$

$$Sh_x = -\frac{x}{(C_w - C_\infty)}\frac{\partial C}{\partial z} \text{ at } z = 0, \quad (28)$$

$$Nn_x = -\frac{x}{(N_w - N_\infty)}\frac{\partial N}{\partial z} \text{ at } z = 0, \quad (29)$$

$$\mathrm{Re}_x^{-\frac{1}{2}}Nu_x = \frac{-\left(1 + \frac{4}{3}R_d\right)}{1 - S_1}\theta'(0), \quad (30)$$

$$\mathrm{Re}_x^{-\frac{1}{2}}Sh_x = -\left(\frac{1}{1 - S_2}\right)\phi'(0), \quad (31)$$

$$\mathrm{Re}_x^{-\frac{1}{2}}Nn_x = -\left(\frac{1}{1 - S_3}\right)\chi'(0), \quad (32)$$

where $\mathrm{Re}_x = \frac{ax^2}{\nu}$.

3. Results and discussion

This segment is systematized to examine the performance of 3D steady incompressible flow of a Casson nanomaterial model considering bioconvection along with stratifications. The scheme used in this problem is bvp4c.[33–35] The graphical pictures of the following parameters are described. The influences of Pr the Prandtl number and stretching parameter α on $\theta(\eta)$ are interpreted in Fig. 2(a) and (b). From these diagrams, we observe the $\theta(\eta)$ decreases for the higher estimations of Pr the Prandtl number and stretching parameter α. From a mathematical perspective, the Prandtl quantity has contrariwise association with heat diffusivity, and higher estimate of Pr

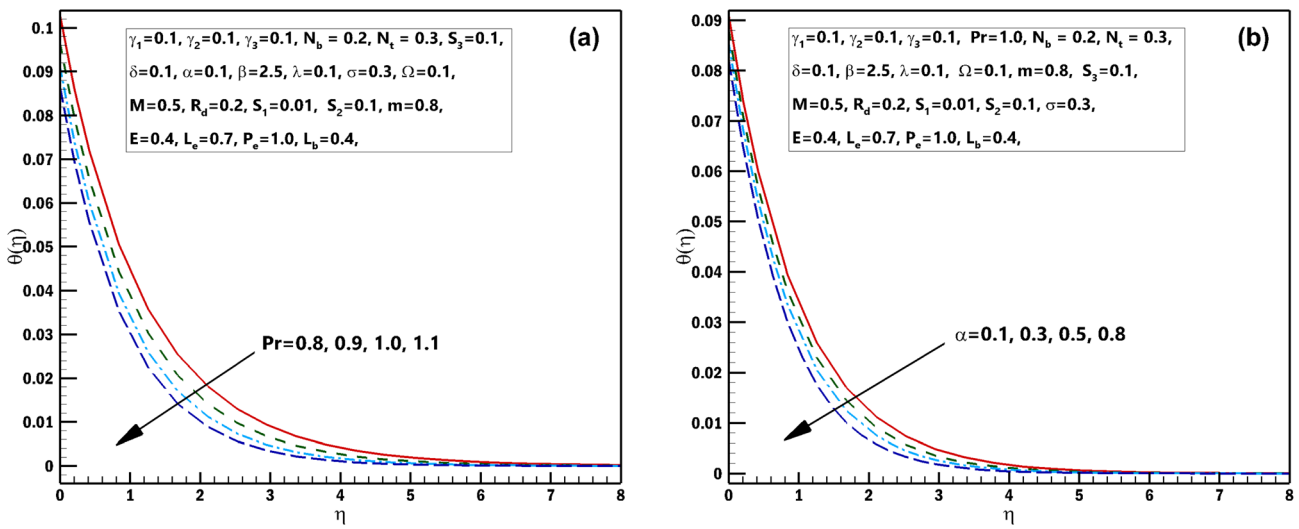

Fig. 2 (a and b) Influence of numerous approximations of [Pr] and [α] on $\theta(\eta)$.

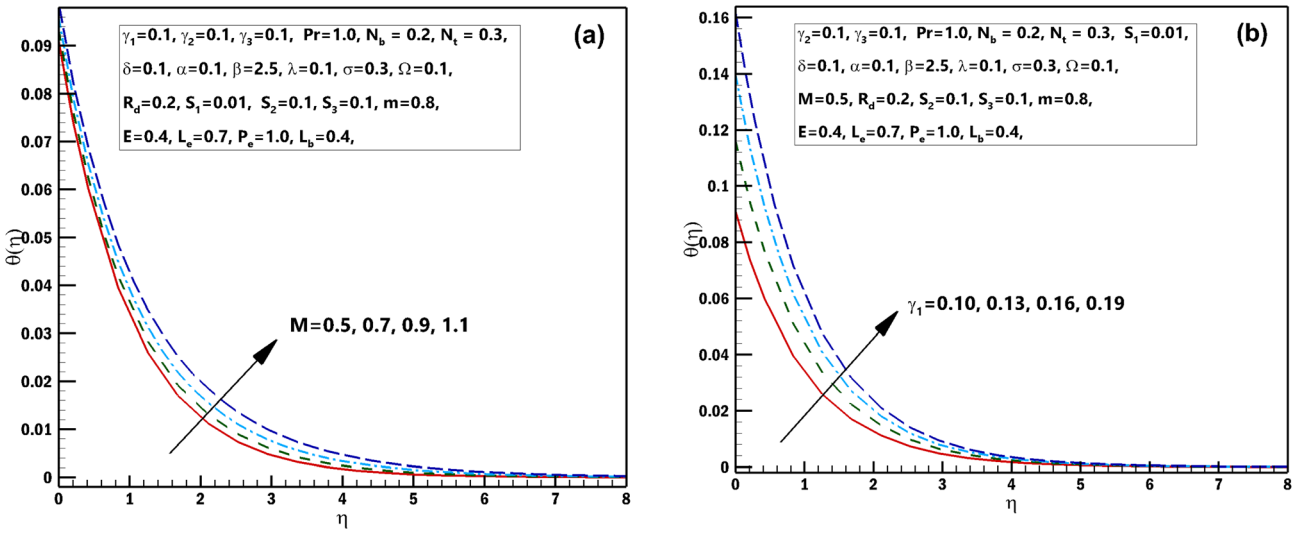

Fig. 3 (a and b) Influence of numerous approximations of [M] and [γ_1] on $\theta(\eta)$.

decay temperature, as shown in the diagram. Fig. 3(a) and (b) displays the results of the magnetic parameter M and γ_1 the thermal Biot number on $\theta(\eta)$. It should be seen from these sketches that both the parameters have a direct relation with the temperature profile. Furthermore, superior estimations of the magnetic parameter M produce more resistive forces between the liquid particles. Consequently, the temperature of the Casson nanofluid is exaggerated. Fig. 4(a) and (b) elucidates the characteristics of the radiation parameter R_d along with the porosity parameter λ on $\theta(\eta)$. It should be perceived from these figures that both the parameters have a direct relation with the temperature profile. Thermal-radiation procedures yield extra heat inside the functioning fluid thus R_d and connected thermal-layer viscosity enhances. Extraordinary development in thermal-radiation, R_d improves the temperature field. The features of Lewis number L_e and S_2 mass stratified variable on $\phi(\eta)$ are displayed in Fig. 5(a) and (b). From these figures, we perceive that $\phi(\eta)$ decreases with growing values of both the parameters. It is perceived that for prevailing estimates of the concentration of Casson nanofluid L_e contracts. In fact, owing to the reverse fraction amongst L_e and Brownian diffusion coefficient displays a decline in the diffusion coefficient, consequently L_e drops. The outcomes of the magnetic parameter M and the reaction constant σ on $\phi(\eta)$ are exhibited in Fig. 6(a) and (b). These figures exhibited that both the parameters are inversely related to the concentration profile. The influences of the Brownian motion parameter N_b and stretching parameter α on $\phi(\eta)$ are displayed in Fig. 7(a) and (b). As of these diagrams, we identify that the concentration profile decays with growing estimates of both the parameters. The developed flying nano-particle collisions through greater N_b upshot in conflict to species diffusion, which reduces $\phi(\eta)$ besides a feeble thickness

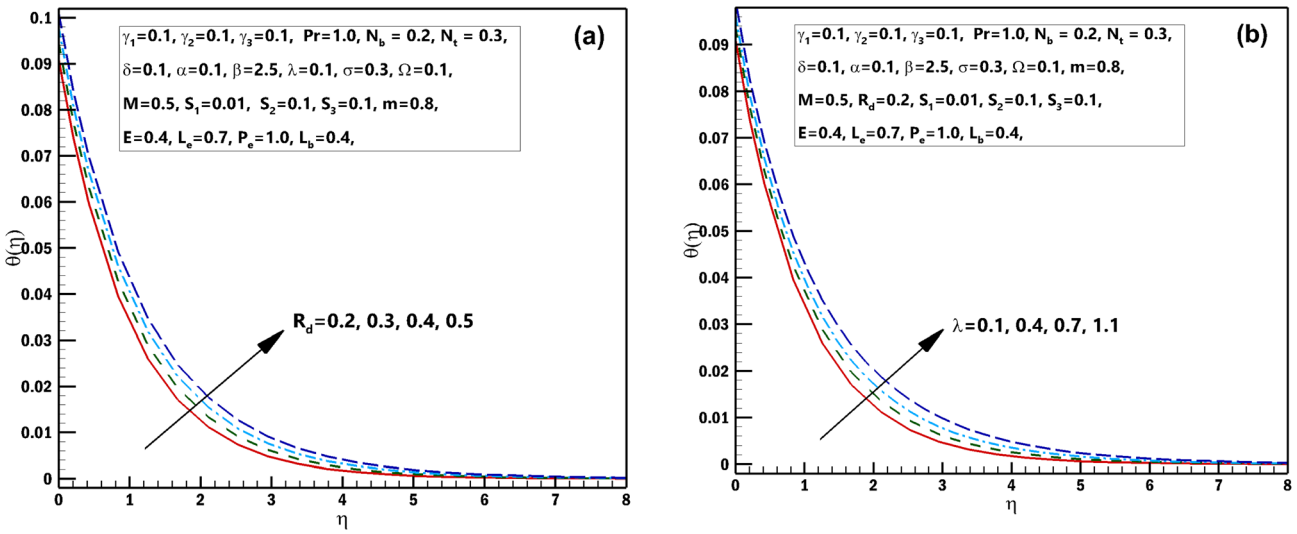

Fig. 4 (a and b) Influence of numerous approximations of [R_d] and [λ] on $\theta(\eta)$.

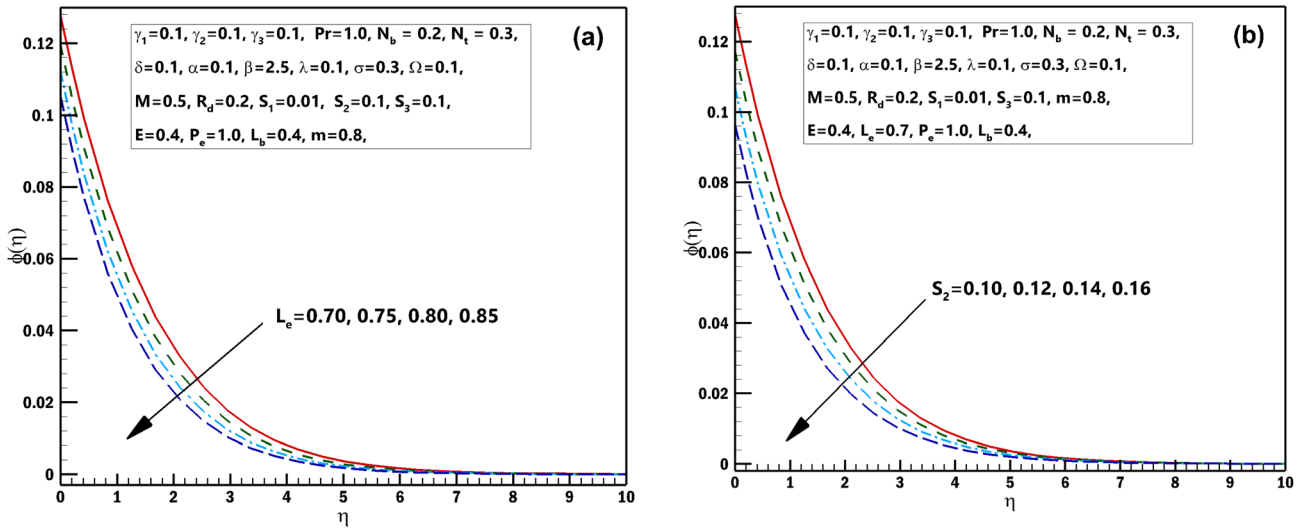

Fig. 5 (a and b) Influence of numerous approximations of [L_e] and [S_2] on $\phi(\eta)$.

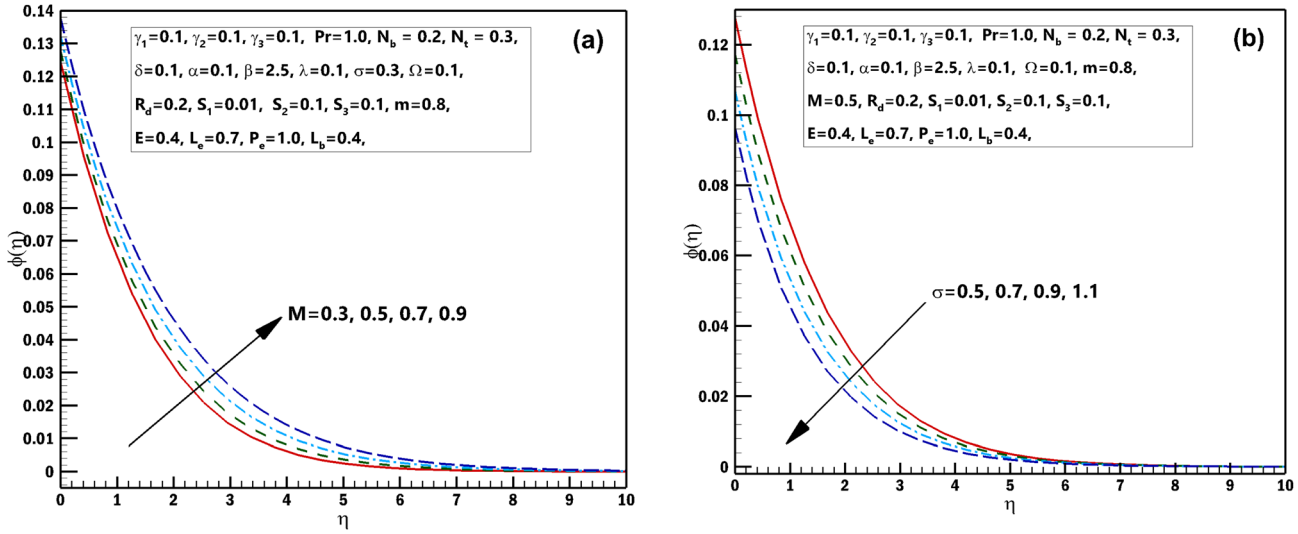

Fig. 6 (a and b) Influence of numerous approximations of [M] and [σ] on $\phi(\eta)$.

of the concentration layer. Fig. 8(a) and (b) express the significance of the thermophoresis parameter N_t and γ_2 concentration Biot number on $\phi(\eta)$. These figures display that both the parameters have a direct relation with concentration profile. From the mathematical viewpoint, the mass transferal coefficient declines as soon as γ_2 is augmented. Hence, $\phi(\eta)$ for superior assessment of γ_2. Furthermore, amplifying thermophoretic influence N_t encourages the immigration of nanomaterial underneath the current rise in the way of cooler regions then this advances the concentration of nanomaterial intended for such purpose produces a sophisticated boundary layer thickness. Fig. 9(a) and (b) illuminate the inspirations of the activation energy E and the porosity parameter λ possessions on $\phi(\eta)$. Fig. 10(a) and (b) interprets the impacts of the stretching parameter α and Ω the microorganism difference parameter distinction on $\chi(\eta)$. These figures revealed that both the parameters have the same contradictory relation with concentration profile. These figures revealed that both the parameters have the same contradictory relation with microorganism profile. Fig. 11(a) and (b) exhibit the effects of γ_3 microorganisms Biot number and S_3 the microorganisms stratified variable on $\chi(\eta)$. These figures display that both the parameters are inversely related with microorganism profile. Fig. 12(a) and (b) demonstrate the significances of P_e Peclet number along with L_b bioconvection Lewis number on $\chi(\eta)$. These figures demonstrated that the microorganism profile decreases for improving estimates of P_e Peclet number along with L_b bioconvection Lewis number. By improving the Peclet number we found a decrease in the micro-organism profile. Actually this parameter narrates the advection rate of microorganisms boosted due to the flow in the direction of the rate of $\chi(\eta)$ diffusion. Naturally Peclet number is related through

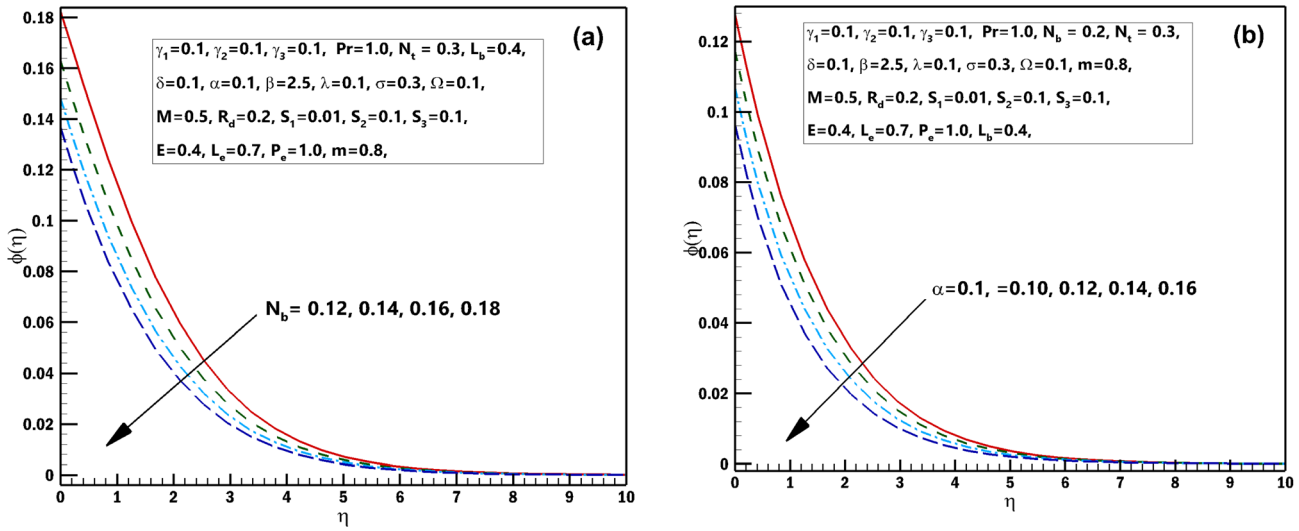

Fig. 7 (a and b) Influence of numerous approximations of [N_b] and [α] on $\phi(\eta)$.

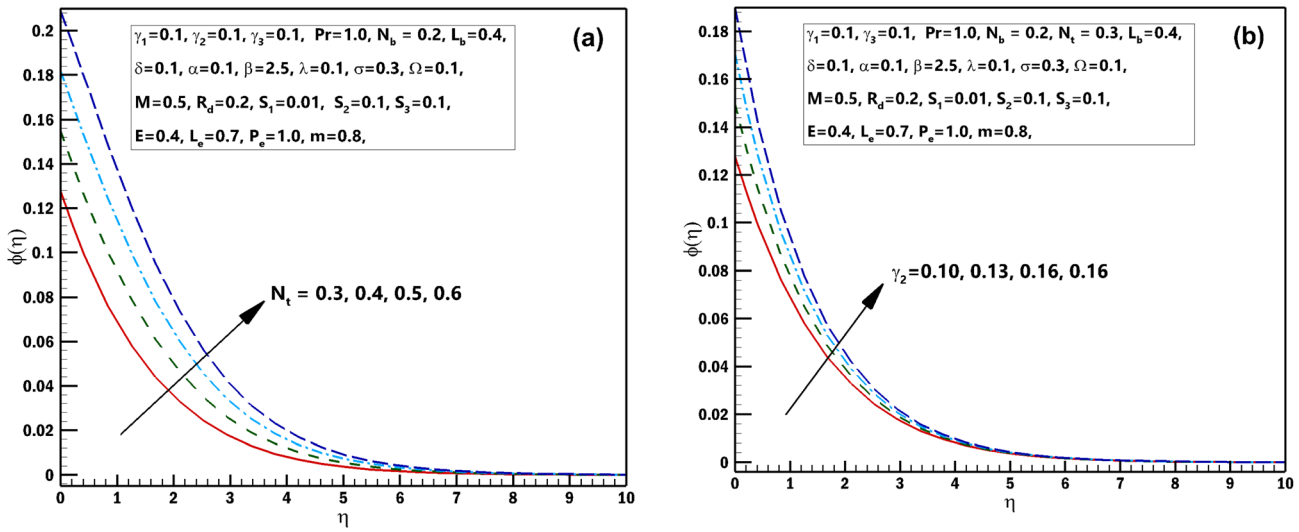

Fig. 8 (a and b) Influence of numerous approximations of [N_t] and [γ_2] on $\phi(\eta)$.

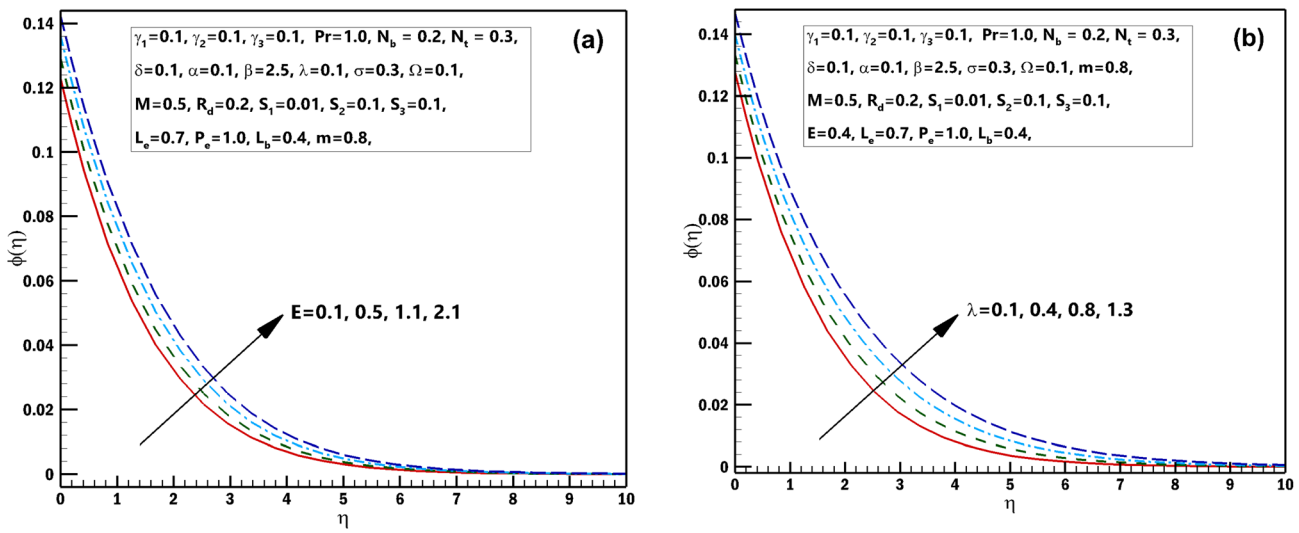

Fig. 9 (a and b) Influence of numerous approximations of [E] and [λ] on $\chi(\eta)$.

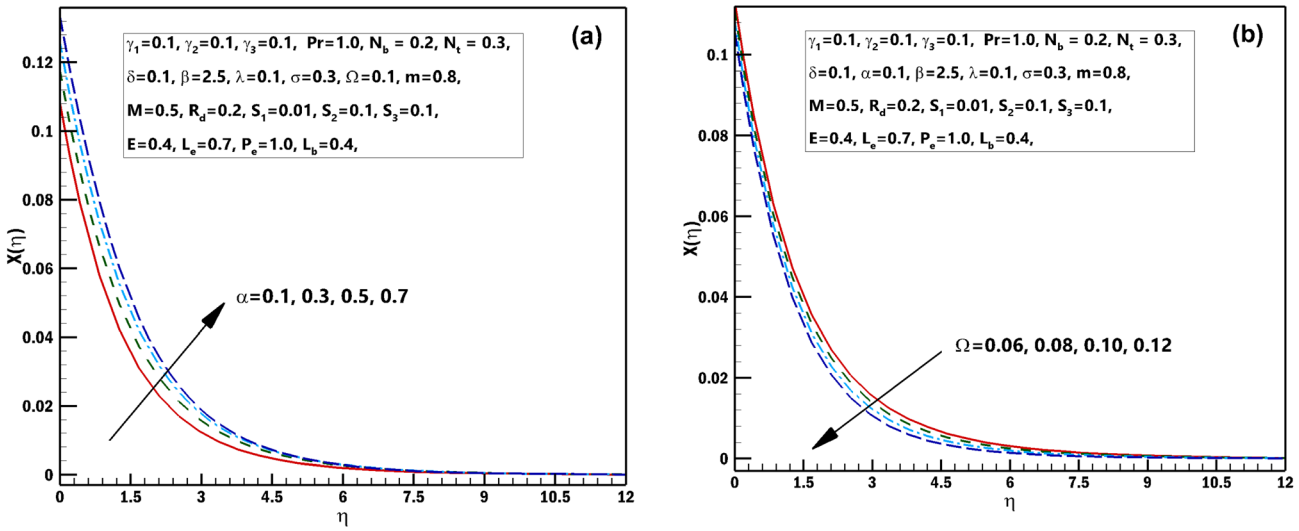

Fig. 10 (a and b) Influence of numerous approximations of [α] and [Ω] on $\chi(\eta)$.

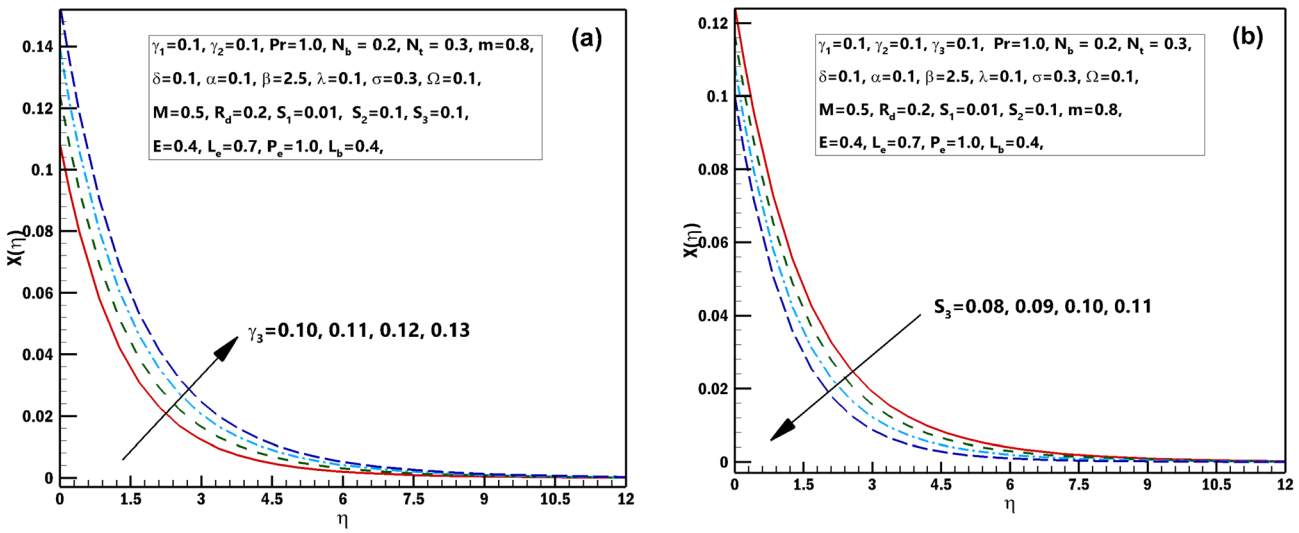

Fig. 11 (a and b) Influence of numerous approximations of [γ_3] and [S_3] on $\chi(\eta)$.

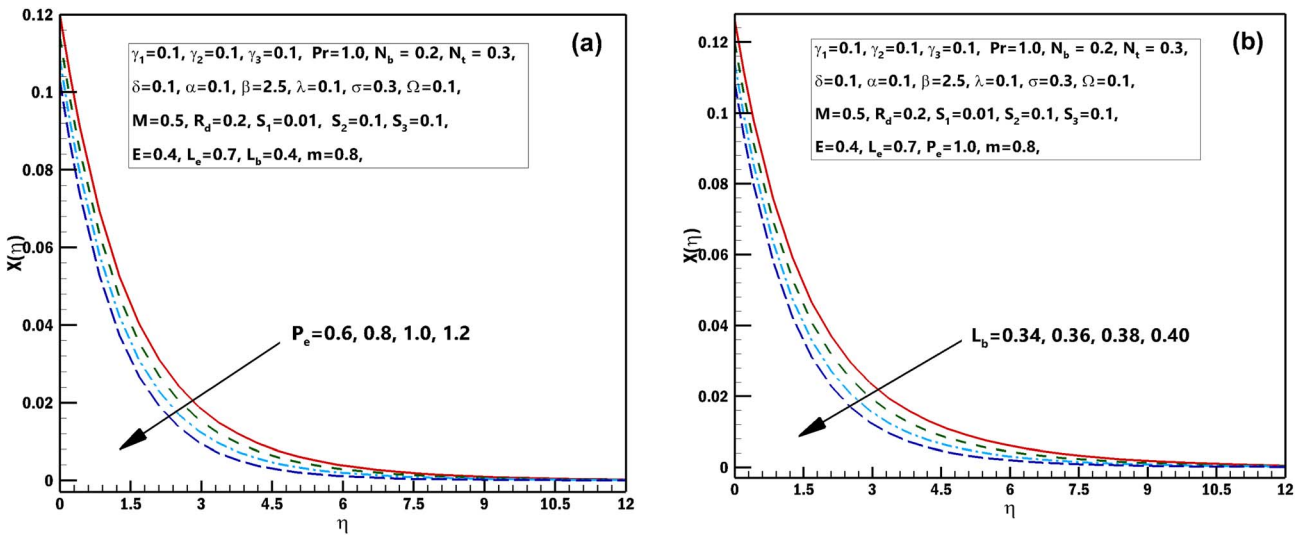

Fig. 12 (a and b) Influence of numerous approximations of [P_e] and [L_b] on $\chi(\eta)$.

Table 1 Comparison of M for $C_{fx}\mathrm{Re}_x^{0.5}$ when $\beta = \infty$, $\lambda = \alpha = 0$

	$C_{fx}\mathrm{Re}_x^{0.5}$		
M	Akbar *et al.*[36]	Waqas *et al.*[26]	Present bvp4c
0	1	1	1
0.3		1.0440	1.04402
0.5	1.11803	1.1180	1.11801
0.7		1.2206	1.22064
1.0	1.41421	1.4141	1.41413

Table 2 $\mathrm{Re}^{-\frac{1}{2}}\mathrm{Nu}_x$ for different Pr, γ_1, S_1 and R_d

Pr	γ_1	S_1	R_d	bvp4c technique
1.0	0.1	0.02	0.1	0.115020
1.1				0.115607
1.2				0.116114
1.3				0.116557
	0.2			0.210228
	0.3			0.290457
	0.4			0.359029
	0.5			0.418268
		0.03		0.116458
		0.04		0.117172
		0.05		0.117900
		0.06		0.118644
			0.2	0.115071
			0.3	0.126694
			0.4	0.138244
			0.5	0.149725

convection heat transference procedures and also usually designates the heat transport. This parameter conspicuously changes flow designs of $\chi(\eta)$. The greater value of Peclet number corresponds to enhanced speediness of swimming that declines their concentration. The converse influence is perceived at subordinate Peclet number and their growth relaxed acquiescent sophisticated concentrations. At this point, the noteworthy decrease of microorganisms distribution function $\chi(\eta)$ is achieved in contrast to better involvements of bioconvection Lewis number L_b, which is reciprocal to mass diffusivity of microorganisms.

Table 1 reports a brilliant comparison with those of Akbar *et al.*[36] and Waqas *et al.*[26] for various values of M on $C_{fx}\mathrm{Re}_x^{0.5}$. Table 2, estimates the dissimilarities in $\mathrm{Re}^{-\frac{1}{2}}\mathrm{Nu}_x$ developing parameters Pr, γ_1, S_1 and R_d. It is inspected that the deviance of $\mathrm{Re}^{-\frac{1}{2}}\mathrm{Nu}_x$ growths by increasing the approximations of parameters Pr, γ_1, S_1 and R_d. Table 3, scrutinizes the variations in $\mathrm{Sh}_x\mathrm{Re}_x^{-\frac{1}{2}}$ with several evaluations of captivating parameters N_t, L_e, N_b and γ_2. It can be perceived that by growing the parameters L_e, N_b and γ_2 an intensification in $\mathrm{Sh}_x\mathrm{Re}_x^{-\frac{1}{2}}$ is originated. A contradictory performance can be appreciated N_t. The different values of Ω, L_b, P_e and S_3 against $\mathrm{Nn}_x\mathrm{Re}_x^{-\frac{1}{2}}$ are demonstrated in Table 4, we noticed that $\mathrm{Nn}_x\mathrm{Re}_x^{-\frac{1}{2}}$ decreases by refining S_3. While $\mathrm{Nn}_x\mathrm{Re}_x^{-\frac{1}{2}}$ increases for the parameters Ω, L_b, P_e.

Table 3 $\mathrm{Sh}_x\mathrm{Re}_x^{-\frac{1}{2}}$ for different N_t, L_e, N_b and γ_2

N_t	L_e	N_b	γ_2	bvp4c technique
0.3	0.4	0.1	0.3	0.0807154
0.4				0.0780301
0.5				0.0753527
0.6				0.0726832
	0.5			0.0763572
	0.6			0.0788308
	0.7			0.0807154
	0.8			0.0822065
		0.2		0.0822065
		0.3		0.0846472
		0.4		0.0858676
		0.5		0.0865998
			0.4	0.258338
			0.5	0.301387
			0.6	0.339054
			0.7	0.372288

Table 4 $\mathrm{Nn}_x\mathrm{Re}_x^{-\frac{1}{2}}$ for different Ω, L_b, P_e and S_3

Ω	L_b	P_e	S_3	bvp4c technique
0.2	0.3	1.0	0.01	0.0726217
0.3				0.0738469
0.4				0.075072
0.5				0.0762972
	0.4			0.0726217
	0.5			0.0745206
	0.6			0.0759949
	0.7			0.0771863
		1.1		0.0729859
		1.2		0.0733404
		1.3		0.0736855
		1.4		0.0740217
			0.02	0.0804444
			0.03	0.0794543
			0.04	0.0784678
			0.05	0.0774847

4. Major findings

The research analysed the implications of bioconvection, magnetic field, Brownian motion, thermophoresis diffusion, and Arrhenius activation energy on Casson's fluid flow in the existence of nanoparticles along with microorganisms. We examined thermal and solutal stratification boundary conditions for this study. Furthermore, thermal radiation was exploited to designate the heat transportation mechanism. An efficient numerical technique was utilized to solve the model equations and verify the experimental work. Numerical experiments for parametric analysis were carried out. The performance of temperature, mass concentration, and microorganism was revealed by using graphs and tables. The results can be outlined as follows:

1. The temperature field of Casson fluid rises for greater approximations of R_d the radiation parameter and the porosity parameter λ.

2. By improving the values of Prandtl number Pr and stretching parameter α decay the Casson fluid temperature.

3. The Lewis number L_e and S_2 mass stratified variable have diminishing performance for the concentration field.

4. The concentration field has a contradictory tendency with the deviation of thermophoresis N_t and reaction constant σ in the flow of Casson nanofluid.

5. The Peclet number P_e and bioconvection Lewis number L_b have decreasing behavior for microorganism profiles.

6. We observed a conflicting behavior for γ_3 microorganisms Biot number, and S_3 the microorganisms stratified variable in the Casson microorganism profile.

Abbreviations

(x, y, z)	Coordinate axis (m)
$(\rho c)_f$	Fluid's heat capacity (J K^{-1})
(u, v, w)	velocity coordinates (m s^{-1})
B	Magnetic induction (kg s^{-2} m^{-2})
D_T	Thermophoresis diffusion coefficient (m^2 s^{-1})
C	Fluid concentration profile (kg m^{-3})
α_1	Thermal diffusivity (m^2 s^{-1})
T	Fluid temperature (K)
c_p	Specific heat capacity (J kg^{-1} K^{-1})
ν	Kinematic viscosity (m^2 s^{-1})
σ^{**}	Electrical conductivity (S m^{-1})
D_B	Brownian diffusion coefficient (m^2 s^{-1})
k^*	Mean absorption coefficient (m^{-1})
ρ	Fluid density (kg m^{-3})
σ^*	Stefan–Boltzmann constant (W m^{-2} K^{-4})
k	Thermal conductivity (W m^{-1} K^{-1})
C_∞	Ambient concentration (kg m^{-3})
N_w	Motile gyrotactic microorganism surface
T_∞	Ambient temperature (K)
T_w	Wall temperature (K)
q_r	Radiative heat flux (kg s^{-3})
W_c	Maximum cell swimming speed (m s^{-1})
D_m	Diffusivity of microorganism (m^2 s^{-1})
U_w	Stretching velocity (m s^{-1})
Nn_x	Local density of microbe
E_a	Wall shear stress
d_1, d_2, d_3	Positive constants
N_b	Brownian motion parameter
θ	Dimensionless temperature
K	Porous medium permeability
σ	Chemical reaction parameter
η	Non-dimensional variable
N	Gyrotactic microorganism
β	Casson fluid parameters
Nu_x	Nusselt number
N_∞	Ambient motile organism density
C_w	Concentration on elastic sheet surface
λ	Porosity parameter
γ_3	Microorganism stratification Biot number
L_e	Lewis number
γ_2	Mass stratification Biot number
S_3	Microorganism stratification parameter
L_b	Bioconvection Schmidt number
S_1	Thermal stratification parameter
Sh_x	Local Sherwood number
γ_1	Thermal stratification Biot number
δ	Temperature difference parameter
S_2	Mass stratification parameter
Pr	Prandtl number
P_e	Bio-convection Peclet number
Ω	Microorganisms difference parameter
N_b	Brownian movement parameter
R_d	Thermal radiation parameter
M	Magnetic parameter
α	Stretching ratio parameter
χ	Dimensionless microorganism field
N_t	Thermophoresis parameter
E	Activation energy

Conflicts of interest

There are no conflicts to declare.

Acknowledgements

The authors extend their appreciation to the Deanship of Scientific Research at King Khalid University, Abha, Saudi Arabia for funding this work through Large Groups Project under grant number RGP.2/329/44.

References

1 S. U. Choi and J. A. Eastman, *Enhancing thermal conductivity of fluids with nanoparticles*, Argonne. National. Lab., IL, United States, 1995.

2 J. Buongiorno, *Convective transport in nanofluids*, 2006, pp. 240–250.

3 E. Abu-Nada and H. F. Oztop, Effects of inclination angle on natural convection in enclosures filled with Cu-water nanofluid, *Int. J. Heat Fluid Flow*, 2009, **30**, 669–678.

4 M. Shahzad, H. Sun, F. Sultan, W. A. Khan, M. Ali and M. Irfan, Transport of radiative heat transfer in dissipative Cross nanofluid flow with entropy generation and activation energy, *Phys. Scr.*, 2019, **94**, 115224.

5 M. I. Khan, S. A. Khan, T. Hayat, M. Waqas and A. Alsaedi, Modeling and numerical simulation for flow of hybrid nanofluid (SiO2/C3H8O2) and (MoS2/C3H8O2) with entropy optimization and variable viscosity, *Int. J. Numer. Methods Heat Fluid Flow*, 2020, **22**, 3939–3955.

6 S. A. Khan, T. Hayat, A. Alsaedi and B. Ahmad, Melting heat transportation in radiative flow of nanomaterials with irreversibility analysis, *Renewable Sustainable Energy Rev.*, 2021, **140**, 110739.

7 M. Ali, F. Sultan, W. A. Khan and M. Shahzad, Exploring the physical aspects of nanofluid with entropy generation, *Appl. Nanosci.*, 2020, **10**, 3215–3225.

8 S. A. Khan, T. Hayat and A. Alsaedi, Thermal conductivity performance for ternary hybrid nanomaterial subject to entropy generation, *Energy Rep.*, 2022, **8**, 9997–10005.

9 S. A. Khan, T. Hayat and A. Alsaedi, Entropy optimization for nanofluid flow with radiation subject to a porous medium, *J. Pet. Sci. Eng.*, 2022, **217**, 110864.
10 N. Anjum, W. A. Khan, M. Ali, I. Hussain, M. Waqas and M. Irfan, Thermal performance analysis of Sutterby nanoliquid subject to melting heat transportation, *Int. J. Mod. Phys. B*, 2022, 2350185.
11 J. R. Platt, Bioconvection Patterns in Cultures of Free-Swimming Organisms, *Science*, 1961, **133**, 1766–1767.
12 A. V. Kuznetsov, The onset of nanofluid bioconvection in a suspension containing both nanoparticles and gyrotactic microorganisms, *Int. Commun. Heat Mass Transfer*, 2010, **37**, 1421–1425.
13 Usman, M. M. Bhatti, A. Ghaffari and M. H. Doranehgard, The role of radiation and bioconvection as an external agent to control the temperature and motion of fluid over the radially spinning circular surface: a theoretical analysis via Chebyshev spectral approach, *Math. Methods Appl. Sci.*, 2023, 11523–11540.
14 Y. M. Chu, S. Jakeer, S. R. R. Reddy, M. L. Rupa, Y. Trabelsi, M. I. Khan, H. A. Hejazi, B. M. Makhdoum and S. M. Eldin, Double diffusion effect on the bio-convective magnetized flow of tangent hyperbolic liquid by a stretched nano-material with Arrhenius Catalysts, *Case Stud. Therm. Eng.*, 2023, **44**, 102838.
15 N. Anjum, W. A. Khan, M. Azam, M. Ali, M. Waqas and I. Hussain, Significance of bioconvection analysis for thermally stratified 3D Cross nanofluid flow with gyrotactic microorganisms and activation energy aspects, *Therm. Sci. Eng. Prog.*, 2023, **38**, 101596.
16 W. A. Khan, M. Irfan, M. Khan, A. S. Alshomrani, A. K. Alzahrani and M. S. Alghamdi, Impact of chemical processes on magneto nanoparticle for the generalized burgers fluid, *J. Mol. Liq.*, 2017, **234**, 201–208.
17 T. Hayat, S. A. Khan, A. Alsaesi and H. M. Fardoun, Heat transportation in electro- magnetohydrodynamic flow of Darcy-Forchheimer viscous fluid with irreversibility analysis, *Phys. Scr.*, 2020, **95**, 105214.
18 S. A. Khan, T. Hayat and A. Alsaedi, Simultaneous features of Soret and Dufour in entropy optimized flow of Re iner-Rivlin fluid considering thermal radiation, *Int. Commun. Heat Mass Transfer*, 2022, **137**, 106297.
19 S. A. Khan, T. Hayat and A. Alsaedi, Numerical study for entropy optimized radiative unsteady flow of Prandtl liquid, *Fuel*, 2022, **319**, 123601.
20 S. A. Khan, T. Hayat, A. Alsaedi and M. S. Alhodaly, Thermal analysis for radiative flow of Darcy–Forchheimer nanomaterials subject to entropy generation, *J. Comput. Des. Eng.*, 2022, **9**, 1756–1764.
21 M. Irfan, Influence of thermophoretic diffusion of nanoparticles with Joule heating in flow of Maxwell nanofluid, *Numer. Methods Part. Differ. Equ.*, 2023, **39**(2), 1030–1041.
22 M. Irfan, *Energy transport phenomenon via Joule heating and aspects of Arrhenius activation energy in Maxwell nanofluid*, Waves Random Complex media, 2023, DOI: **10.1080/17455030.2023.2196348**.
23 M. M. Bhatti, A. Shahid, L. E. Sarris and O. A. Beg, Spectral relaxation computation of Maxwell fluid flow from a stretching surface with quadratic convection and non-Fourier heat flux using Lie symmetry transformations, *Int. J. Mod. Phys. B*, 2023, **37**, 2350082.
24 M. M. Bhatti, O. A. Beg, R. Ellahi and T. Abbas, Natural Convection Non-Newtonian EMHD Dissipative Flow Through a Microchannel Containing a Non-Darcy Porous Medium: Homotopy Perturbation Method Study, *Qual. Theory Dyn. Syst.*, 2022, **21**, DOI: **10.1007/s12346-022-00625-7**.
25 N. Casson, A flow equation for the pigment oil suspension of the printing ink type, *Rheol. Disperse Syst.*, 1959, 84–102.
26 M. Waqas, W. A. Khan, A. A. Pasha, N. Islam and M. M. Rahman, Dynamics of bioconvective Casson nanoliquid from a moving surface capturing gyrotactic microorganisms, magnetohydrodynamics and stratifications, *Therm. Sci. Eng. Prog.*, 2022, **36**, 101492.
27 A. Shahid, W. Wei, M. M. Bhatti, O. A. Bég and T. A. Bég, Mixed convection Casson polymeric flow from a nonlinear stretching surface with radiative flux and non-Fourier thermal relaxation effects: Computation with CSNIS, *ZAMM*, 2023, **103**(10), e202200519.
28 U. Ali, M. Irfan, N. S. Akbar, K. U. Rehman and W. Shatanawi, Dynamics of Soret–Dufour effects and thermal aspects of Joule heating in multiple slips Casson–Williamson nanofluid, *Int. J. Mod. Phys. B*, 2023, DOI: **10.1142/S0217979224502060**.
29 J. Qing, M. M. Bhatti, M. A. Abbas, M. M. Rashidi and M. E. S. Ali, Entropy Generation on MHD Casson Nanofluid Flow over a Porous Stretching/Shrinking Surface, *Entropy*, 2016, **18**(4), 123.
30 K. Bhattacharyya, MHD Stagnation-Point Flow of Casson Fluid and Heat Transfer over a Stretching Sheet with Thermal Radiation, *J. Thermodyn.*, 2013, **2013**, 169674.
31 G. Mahanta and S. Shaw, 3D Casson fluid flow past a porous linearly stretching sheet with convective boundary condition, *Alexandria Eng. J.*, 2015, **54**, 653–659.
32 U. Ali and M. Irfan, Thermal aspects of multiple slip and Joule heating in a Casson fluid with viscous dissipation and thermo-solutal convective conditions, *Int. J. Mod. Phys. B*, 2023, **37**, 2350043.
33 M. Khan, M. Irfan, W. A. Khan and A. S. Alshomrani, A new modeling for 3D Carreau fluid flow considering nonlinear thermal radiation, *Results Phys.*, 2017, **7**, 2692–2704.
34 Z. Hussain, W. A. Khan, T. Muhammad, H. A. Alghamdi, M. Ali and M. Waqas, Dynamics of gyrotactic microorganisms for chemically reactive magnetized 3D Sutterby nanofluid flow comprising non-uniform heat sink-source aspects, *J. Magn. Magn. Mater.*, 2023, **587**, 170798.
35 Z. Hussain, M. M. Alam, A. A. Pasha, W. A. Khan, M. Ali and A. I. Khan, Gyrotactic microorganisms analysis for radiative 3D Carreau nanofluid flow configured by activation energy and viscous dissipation, *Therm. Sci. Eng. Prog.*, 2023, **42**, 101898.
36 N. S. Akbar, S. Nadeem, R. U. Haq and Z. H. Khan, Numerical solutions of Magnetohydrodynamic boundary layer flow of tangent hyperbolic fluid towards a stretching sheet, *Indian J. Phys.*, 2013, **87**, 1121–1124.